Geophysical Research Letters

Key Points:
- Submicrosecond time-resolved spectra of lightning-like discharges are presented for the first time
- Some evidence points to slight non-LTE conditions right behind the shock front in posttrigger submicrosecond times
- Optical thickness goes from thin (pretrigger times) to thick (submicrosecond) and back to thin (few microseconds)

Supporting Information:
- Supporting Information S1

Submicrosecond Spectroscopy of Lightning-Like Discharges: Exploring New Time Regimes

N. Kieu[1], F. J. Gordillo-Vázquez[1] (iD), M. Passas[1] (iD), J. Sánchez[1], F. J. Pérez-Invernón[1,2] (iD), A. Luque[1] (iD), J. Montanyá[3] (iD), and H. Christian[4]

[1]Instituto de Astrofísica de Andalucía (IAA-CSIC), Granada, Spain, [2]Deutsches Zentrum für Luft- und Raumfahrt, Institut für Physik der Atmosphäre, Oberpfaffenhofen, Germany, [3]Department of Electrical Engineering, Universitat Politécnica de Catalunya, Terrassa, Spain, [4]Earth System Science Center, University of Alabama in Huntsville, Huntsville, AL, USA

Abstract Submicrosecond ($0.476\,\mu s$ per frame with an exposure time of $160\,ns$) high-resolution ($0.38\,nm$) time-resolved spectra of laboratory-produced lightning-like electrical discharges have been recorded for the first time within the visible spectral range (645–665 nm). The spectra were recorded with the GrAnada LIghtning Ultrafast Spectrograph (GALIUS), a high-speed imaging spectrograph recently developed for lightning research in the IAA-CSIC. Unprecedented spectral time dynamics are explored for meter long laboratory electrical discharges produced with a 2.0 MV Marx generator. The maximum electron density and gas temperature measured in a timescale of $\leq 0.50\,\mu s$ (160 ns) were, respectively, $\simeq 10^{18}\,cm^{-3}$ and $\simeq 32,000\,K$. Overpressure in the lightning-like plasma channel, black-body dynamics, and self-absorption in spectral lines were investigated.

Plain Language Summary Lightning are extremely rapid and violent atmospheric electricity events taking place inside thunderclouds and between thunderclouds and the ground. Investigation of the fundamental properties of different types of lightning and lightning leaders can help to deepen our understanding on lightning propagation dynamics (stepping) and how lightning can produce high-energy pulses of X-ray or pulses of even higher energy (the so-called terrestrial gamma-ray flashes). Time-resolved optical emission spectroscopy is an ideal diagnostic technique to remotely study the fast temporal dynamics of lightning. The fastest spectroscopic techniques used to date were able to achieve microsecond timescales. We present the first study exploring submicrosecond time regimes using the GrAnada LIghtning Ultrafast Spectrograph (GALIUS), a high-speed imaging spectrograph recently developed for lightning research at the IAA-CSIC.

1. Introduction

Time-resolved lightning spectroscopy started in 1962 when Salanave et al. (1962) first developed slitless spectroscopic techniques (time-resolved flash spectra) to investigate time-integrated spectra of individual strokes within a lightning flash with time and spectral resolutions of, respectively, 20 ms and about 0.2 nm. The millisecond timescale of Salanave's technique allowed for the first time to spectroscopically monitor return stroke continuing currents (Orville & Salanave, 1970) that were earlier proposed (McEachron & Hagenguth, 1942) to produce forest fires, which was confirmed in 1967 (Fuquay et al., 1967).

The first successful attempt to time resolve the spectra of individual return strokes in cloud-to-ground (CG) lightning was not performed with spectrometers but with a set of narrowband interference filters (of selected wavelengths) and photomultiplier tubes with 5 µs time resolution (Krider, 1965a, 1965b). Krider (1965b) carried out, using a silicon photodiode (with flat spectral response between 400 and 1,000 nm), the highest time resolution (0.2 µs) study to date of the relative light intensities of five leader steps immediately before a return stroke in CG lightning. Krider was able to capture the leader stepping time dynamics observing that a typical step rises from zero to peak in about 1 µs, falls to half peak in 1 to 2 µs, and then decays slowly until next step occurs (Krider, 1974; Orville, 1977).

In a series of papers published between 1966 (Orville, 1966a, 1966b) and 1968 (Orville, 1968a, 1968b, 1968c, 1968d), Orville introduced high-speed slitless spectroscopic techniques based on photographic recordings able to achieve time resolutions between 2 and 5 µs with good spectral resolution (1 nm) (Orville, 1968a, 1968b). This technique allowed time-resolved spectroscopic investigations of return strokes (Orville,

1968a, 1968b) and stepped leaders (Orville, 1968d)—in the range 560 to 660 nm—including a quantitative analysis to derive the electron temperature and electron density by methods first proposed in 1963 (Prueitt, 1963) and 1964 (Uman & Orville, 1964), respectively. Later in 1975, dart leaders preceding subsequent return strokes were also spectroscopically investigated with a time resolution of 10 μs (with exposure time of ≃9 μs) in the range from 395 to 510 nm (Orville, 1975). Both the return stroke and stepped leader spectra exhibited neutral and singly ionized atom optical emissions, but neither molecular emissions nor doubly ionized atom emissions were detected (Orville, 1968a, 1968d). The characteristic stepping in the leader was only exhibited in singly ionized emissions within the 528 to 680 nm range of spectra recorded with 20 μs resolution (Orville, 1968d). Time-resolved (10 μs resolution) spectra of dart leaders were found to be dominated by singly ionized emissions within the 399 to 501 nm spectral range (Orville, 1975).

Spectroscopic investigations (with microsecond time resolution) of negative discharges in 10-m-long air gaps were undertaken during the 1970s in Les Renardieres high-voltage laboratory (Les Renardieres Group, 1981).

After the introduction of CCD and CMOS technology in, respectively, the 1980s and 1990s, a new generation of fast and very sensitive camera sensors became available. The availability of new fast and reliable sensors, together with the perfection of artificial initiation of lightning, first demonstrated in 1967 (Newman et al., 1967), led to a renovated interest for lightning spectroscopy research. High time resolution lightning spectroscopy investigations carried out during the second decade of the 21st century have explored spectral features of lightning return strokes (Wang et al., 2014), stepped leaders (Warner et al., 2011), and dart lightning leaders (Cen et al., 2015) within a timescale of 100 μs or longer. It is interesting to note that the modern works by Warner et al. (2011) and Cen et al. (2015)—with expanded spectral ranges of, respectively, 600–1,050 and 400–1,000 nm—were only the second ones on high-speed spectroscopy of stepped and dart leaders after Orville's 1968 and 1975 papers with narrower spectral ranges.

Two recent papers (Walker & Christian, 2017, 2019) discussed the first time-resolved spectra of triggered lightning including high-speed spectroscopic recordings of dart leaders, dart stepped leaders, and return strokes evaluated in two spectral ranges, from 370 to 630 nm and from 630 to 890 nm with a spectral dispersion of 0.26 nm/pixel (spectral resolution between 0.52 and 0.65 nm). In these studies triggered lightning spectra were recorded with 673 kfps (1.5 μs per frame) with exposure times between 0.7 and 1.47 μs. Some new doubly ionized line emissions were found in the 370 to 650 nm range but not in the spectral range from 650 to 850 nm.

The first submicrosecond-resolved (0.476 μs per frame with an exposure time of 0.16 μs) slit spectra with high spectral resolution (0.38 nm) of meter long lightning-like discharges are presented here. Unprecedented spectral time dynamics are shown for lightning-like discharges produced with two different operation modes (lightning [LI] and switching [SI] impulse) of a 2 MV Marx generator. Quantitative analysis of recorded spectra led to measured values of the electron concentration and gas temperature comparable to those found in real lightning due to the extremely high temporal resolution and sensitivity of GALIUS. In addition, our study quantifies the overpressure in the lightning-like channel, the self-absorption (SA) in ionic spectral lines, and the position and speed of the hydrodynamic shock front produced right after electric breakdown leading to lightning-like discharges. We have compared our measured spectra with synthetic spectra calculated for equilibrium air plasmas at atmospheric pressure and have found partial agreement. This, together with the high (>4 km/s) shock front speeds computed, leads us to consider possible slight disruption of equilibrium right behind the shock front in posttrigger submicrosecond times.

2. Instrumentation

The investigations presented here have been carried out with an very fast (2.1 Mfps or 0.476 μs per frame with an exposure time of 160 ns) and high spectral resolution (between 0.29 and 0.75 nm depending on the grating used) spectrograph named GrAnada LIghtning Ultrafast Spectrograph (GALIUS) recently developed by the IAA-CSIC atmospheric electricity group (Passas et al., 2019). A total of 22 possible configurations can be set up with GALIUS, combining 10 interchangeable collector lenses (with focal lengths ranging from 25 to 200 mm) with two different collimator lenses (105 mm with F#4.5 and 50 mm with F#1.2 focal lengths for, respectively, the UV and visible-NIR ranges) and four interchangeable

volume-phase holographic (VPH) grisms for spectral ranges from the near UV (380 nm) to the near IR (850 nm) (Passas et al., 2019).

GALIUS is a compact device that is housed in a portable aluminum box of $1,100 \times 380 \times 230$ mm, which can be bent in elevation from 0° to 50° due to a linear actuator and a telescopic mechanism attached on its fixed base. GALIUS can operate in slit or slitless mode and incorporates a very high speed Photron FASTCAM SAZ camera with a high light-sensitive image CMOS sensor (monochrome ISO 50000) of $1,024 \times 1,024$ of 20 μm square pixels, with 12 bit ADC pixel depth. Finally, GALIUS incorporates a fast photodiode-based photometer for triggering when a threshold of photons is reached (Passas et al., 2019).

For the results presented here, GALIUS is set up in slit mode (50 μm × 3 mm) and operated at 2.1 Mfps using collimator and collector lenses of, respectively, 50 mm (F#1.2) and 30 mm (F#1.5) focal lengths and a grism with a diffraction grating of 1,855 lines/mm with its central wavelength (CWL) in $\simeq$657 nm and a spectral resolution of 0.38 nm.

3. Experimental Setup

During the first half of 2019, a number of experiments were carried with small (several centimeters) sparks and meter long lightning-like discharges produced with, respectively, an electrostatic generator at the IAA-CSIC atmospheric electricity laboratory in Granada (Spain, 940 hPa) and with a 2.0 MV Marx generator at LABELEC in Terrassa (Spain, 1,010 hPa).

Two discharge impulse modes were used at LABELEC with a maximum applied generator voltage of +0.8 MV and a distance between electrodes of $\simeq$1 m. The tip of the grounded electrode was 0.2 m above the floor. GALIUS was pointed to the discharge region just below the upper electrode. The voltage was recorded by a calibrated capacitive voltage divider connected to high-speed digital oscilloscopes. Faraday cages and electromagnetic compatible (EMC) cabinets assured protection against electromagnetic interference.

Each discharge mode has its own positive voltage waveforms (see the supporting information) with distinct rise times. The voltage of the SI was adjusted with a rise time of $\simeq$100 μs exhibiting a fast ($\simeq$0.5 μs) breakdown time. However, the characteristic voltage curve of the LI mode shows a fast ($\simeq$0.5 μs) rise time followed by a short plateau of $\simeq$2–3 μs and the fast ($\simeq$0.5 μs) breakdown time. The currents of the SI and LI modes are both characterized by fast rise times ($\simeq$0.5 μs) but with very different decay times and peak currents (I_{peak}) of, respectively, $\simeq$0.5 μs and $\simeq$0.125 kA (for the SI mode) and tens of microseconds and $\simeq$2.5 kA (for the LI mode). The applied peak voltage and current used to generate the small (4 cm) spark discharge have values of $\simeq$−55 kV and $\simeq$0.350 kA.

The total injected electric energies in each discharge, calculated from their voltage and current, are 81 J (for SI mode), 684 J (for LI mode), and 1.2 J (for the small spark). Figures S1–S3 show the typical voltage and current curve shapes for the discharges investigated in this study.

4. Time-Resolved Spectra

In order to interpret the spectra recorded by GALIUS, we have generated synthetic spectra (shown in the supporting information) based on equilibrium calculations for atmospheric pressure thermal plasmas (see section 6). Calculated spectra include all possible lines of atoms, molecules, singly and doubly ionized ions that can appear in the 645–665 nm spectral range investigated in this study (Kramida et al., 2019). Stark broadening of nonhydrogenic (Bekefi, 1976) and hydrogenic lines (Griem, 1964) are included and convolved with instrumental broadening. In particular, synthetic spectra show the expected relative importance of the different atomic, ionic, and molecular spectral features as a function of the lightning-like channel temperature and serve as a guidance for comparison with the measured spectra.

The 645–665 nm lightning-like synthetic spectra in the supporting information show the presence of six N I neutral lines (648.17, 648.27, 648.37, 648.48, 649.12, and 649.95 nm), two O I neutral lines (645.44 and 645.59 nm), and one H I neutral line (656.27 nm, the so-called H_α line). For the ions we see two singly ionized N II lines (648.20 and 661.05 nm), four singly ionized O II lines (649.58 and 662.73 nm and two lines at 656.52 and 657.11 nm close to the H_α line), and two weak N III doubly ionized emission lines (645.41 and 646.70 nm) not previously detected (Walker & Christian, 2017). Synthetic spectra also predict the presence of

a line at 660.8 nm associated to a vibrational transition ($v' = 6 \rightarrow v'' = 3$) of the first positive system (FPS) of molecular nitrogen (N_2). This molecular spectral feature would only be detectable for temperatures below 12,000 K (see Figure S10). The spectra do not show contamination from the metal electrodes.

Figures 1a and 1b and Figures 1c and 1d show unprecedented spectral time dynamics for meter long lightning-like electrical discharges generated with, respectively, the SI and LI discharge modes of a Marx generator. As shown in Figures 1a and 1c, the SI and LI discharge spectra last for about 12 and 60 μs, respectively. Figures 1b and 1d show different times of the SI and LI discharge spectra where distinct spectral features are visible. The time-resolved spectra of a small (several centimeters long) spark produced with an electrostatic generator are shown in Figures 1e and 1f.

Most recorded spectra exhibit a continuum emission that could be due to different types of continuous radiation sources (Uman, 1963). We found that the contribution of Bremsstrahlung radiation to the continuum is negligible for the measured temperatures and electron densities. Recombination and attachment continuum radiation are of the same order of magnitude as Bremsstrahlung radiation, and cyclotron continuum radiation is unlikely in lightning (Uman, 1963). Thus, by elimination, this leaves black-body radiation as the most probable source of the continuum emission present in the measured spectra. The inclusion of black-body radiation into the calculation of synthetic spectra shows that the detected continuum emission exhibits a shape and magnitude similar to a simulated black-body core at 7,000 K (see the supporting information). The dynamics of the black-body continuum reveals that it is almost zero or very small at pretrigger times (for SI and LI discharges, see Figures 1b and 1d). Then—at early times after triggering—it reaches its larger value, and afterwards, it mildly decreases as time progresses, while the lightning-like channel fades away and reaches ambient pressure.

Three temporal regimes with their own spectral features are clearly distinguishable in the SI and LI lightning-like discharges and in the small spark spectra. First, at early times (≤ 1 μs), ionic emissions dominate. In particular, we can distinguish the 648.20 and 661.05 nm singly ionized N II lines. Less visible, but also present in the submicrosecond timescale of the SI discharge in Figure 1b and the small spark in Figure 1f spectra, are two doubly ionized N III lines at 646.70 nm (more noticeable) and 646.41 nm (less noticeable) to the left of the 648.20 N II ion line (see also synthetic spectra in the supporting information). Finally, very soon after triggering (0.356 and 0.510 μs in, respectively, the SI and spark spectra), we notice that, while the H_α line is not yet clearly emerged, there are two very small humps due to two singly ionized O II lines emitting at 656.52 and 657.11 nm. These two O II lines—hardly distinguishable in the measured spectra—are a bit better appreciated in the synthetic spectra at 32,000 and 33,000 K (see Figures S11 and S13).

The second temporal regime starts after $\simeq 1$ μs and lasts up to $\simeq 2$ μs (in the SI and small spark spectra) and up to $\simeq 10$ μs (in the LI spectra). Here the H_α line is clearly the dominant spectral feature but in concurrence with two N II ion lines at 648.20 and 661.05 nm that softly disappear as time progresses.

Finally, the third temporal regime begins after $\simeq 2$ μs (in the SI and small spark spectra) and after $\simeq 10$ μs (in the LI spectra). This last regime is characterized by the complete prevalence of the H_α line and the replacement of the N II ion line at 648.20 nm by a weak neutral N I emission line at 648.27 nm. The H_α line is the last feature in disappearing at $\simeq 4$ μs (small spark), at $\simeq 12$ μs (SI discharge), and at $\simeq 60$ μs (LI discharge), respectively.

An inspection to the spectra shown in Figure 1 indicates that neither the singly ionized N II (648.20 and 661.05 nm) lines nor the H_α line are self-reversed (causing a central dip in the line). Self-reversion of spectral lines is a manifestation of strong SA and typically occurs in strong resonance lines (involving the ground energy level) and in inhomogeneous (nonuniform) optically thick plasmas. The central dip in self-reversed lines is due to the cold absorbing atoms and/or ions from the outer regions of the lightning-like channel. So, in a first approximation, we can conclude that the lightning-like channel of the discharges investigated in this study is approximately homogenous. In most cases, however, SA produces a height reduction and growth of the spectral line widths that might not be well distinguished from the shape of the different lines in the spectrum (El Sherbini et al., 2005; Parigger et al., 2014).

SA can be important for atomic/ionic resonance lines, lines with low excitation energies of upper levels, and lines with high transition probabilities. We have computed the SA coefficient of the two single ionized N II lines (648.20 and 661.05 nm) appearing in our spectra as a function of the time (see Figure S17). For the
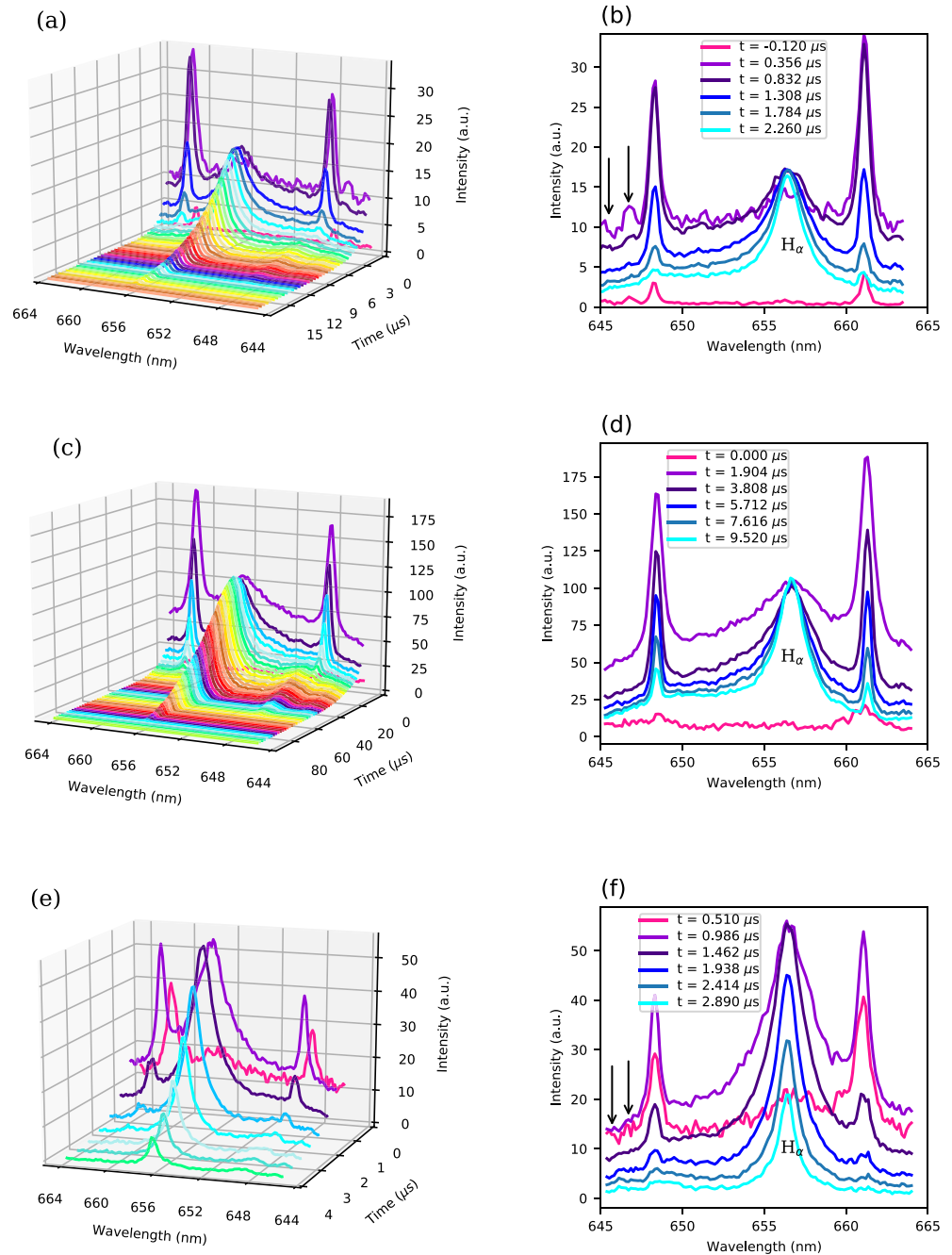
Figure 1. Time-resolved spectra of meter long lightning-like discharges produced with the switching impulse (SI) mode (a, b) and lightning impulse (LI) mode (c, d) of a Marx generator. Panels (e) and (f) show time-resolved spectra of a 4-cm-long spark produced with a small electrostatic generator. The peak intensities and voltages reached in these discharges are 0.125 kA and 0.8 MV for SI mode, 3 kA and 0.8 MV for LI mode, and 0.350 kA and −55.0 kV for the electrostatic spark, respectively. The strong intensities shown correspond to two singly ionized N II lines at 648.20 and 661.05 nm and to the H_α line at 656.27 nm. The panels in the right column show the six initial times for the SI (b) and electrostatic discharges (f) and six selected (not consecutive) instants in the temporal evolution of LI discharges (d). The weak doubly ionized N III emission lines at 645.41 and 646.70 nm marked with arrows can be seen in the very early (submicrosecond) times of spectra in panels (b) and (f). The weak N I neutral line at 648.27 nm is seen (as a soft hump) in the late times of panels (a), (c), and (e).

meter long discharges, we found that the SA coefficient grows toward 1 (complete optically thin) as the lightning-like channel expands and the channel overpressure returns to ambient pressure (see Figures S14–S17). At pretrigger times (only recorded for the SI mode; see Figure S17a), when the channel pressure is nearly ambient, SA is found to be close to 1. The lack of pretrigger times for the LI mode and the small spark prevents SA from exhibiting higher values at the beginning. The estimated SA coefficients refer to both the core channel and the shock front.

5. Electron Density and Temperature

5.1. Electron Density

For electron densities above $\simeq 10^{16}\,\text{cm}^{-3}$, the broadening of spectral lines is controlled by the Stark effect caused by the interaction of charged particles (ions) and emitting atoms within the lightning and/or lightning-like air plasma. Thus we use the Stark broadening of spectral lines to derive the electron density. This method has the advantage of being independent of assumptions about the equilibrium state of the air plasma.

In general, plasma diagnostics using Stark-broadened line profiles considers the full width at half maximum (FWHM) of the line shape as the relevant parameter related to the electron density. However, it is well known that ion dynamics can significantly modify both the width and the shape of certain spectral lines (Gigosos et al., 2003). This effect is especially important for the H_α and H_γ, though it is nearly negligible for the H_β line (Nikiforov et al., 2015). Therefore, as an alternative to the FWHM of the H_α, we evaluate the full width at half area (FWHA) of the H_α line. Thus, when evaluating the H_α line, the FWHA can be considered a more appropriate method for the diagnostics of the electron density in electric discharges forming thermal lightning-like plasmas. The electron concentration is obtained by Gigosos et al. (2003) and Nikiforov et al. (2015):

$$N_e = 10^{17} \times \left(\frac{FWHA}{1.098}\right)^{1.47135} \text{cm}^{-3}. \tag{1}$$

We use the bootstrap method to estimate the error of the FWHA in a single measurement. This allows to derive the error in the electron density as obtained with Equation 1. The key feature of the bootstrap method is subsampling the data with replacement (i.e., if we have N data points, we select among them N points allowing for repetition). In our case we could also drop the repeated values since they do not contribute to the integral we need to calculate to obtain the FWHA (Gigosos et al., 2003).

Figures 2a and 2b show the electron density for, respectively, the meter long SI (red dots) and LI (green dots) discharges and for the short (centimeters) spark (blue dots). No electron density could be retrieved at −0.120 and 0.000 μs (trigger time) for, respectively, the SI and LI discharges due to the negligible H_α signal. The maximum electron density ($\simeq 10^{18}\,\text{cm}^{-3}$) is measured in the LI discharge. The measured electron densities are comparable to those found in natural return strokes (Orville, 1968b) and triggered lightning return strokes with peak currents of 8.1 kA (Walker & Christian, 2019) due to the high temporal resolution and sensitivity of GALIUS.

5.2. Electron Temperature

To calculate the electron temperature from the time-resolved spectra of lightning-like discharges used in this work, we will initially assume the criteria previously established by Prueitt (1963) and Uman (1969), and also recently used by Walker and Christian (2019) for deriving the electron temperature in triggered lightning. In particular, we consider that (a) the channel of the lightning-like discharge is optically thin, (b) the temperature is relatively uniform along the lightning-like channel radial cross section, and (c) thermal equilibrium controls the concentration of the different atoms and ion energy levels emitting light due to spontaneous radiative deexcitation; that is, the density of excited atoms and ions follows Boltzmann's law. We also assume that local thermal equilibrium (LTE) applies so that the derived electron temperature will be equal to the gas temperature.

The electron temperature is calculated from the intensity ratio of the 648.20 and 661.05 nm N II ion lines assuming that the corresponding emitting energy levels are populated following Boltzmann's equilibrium
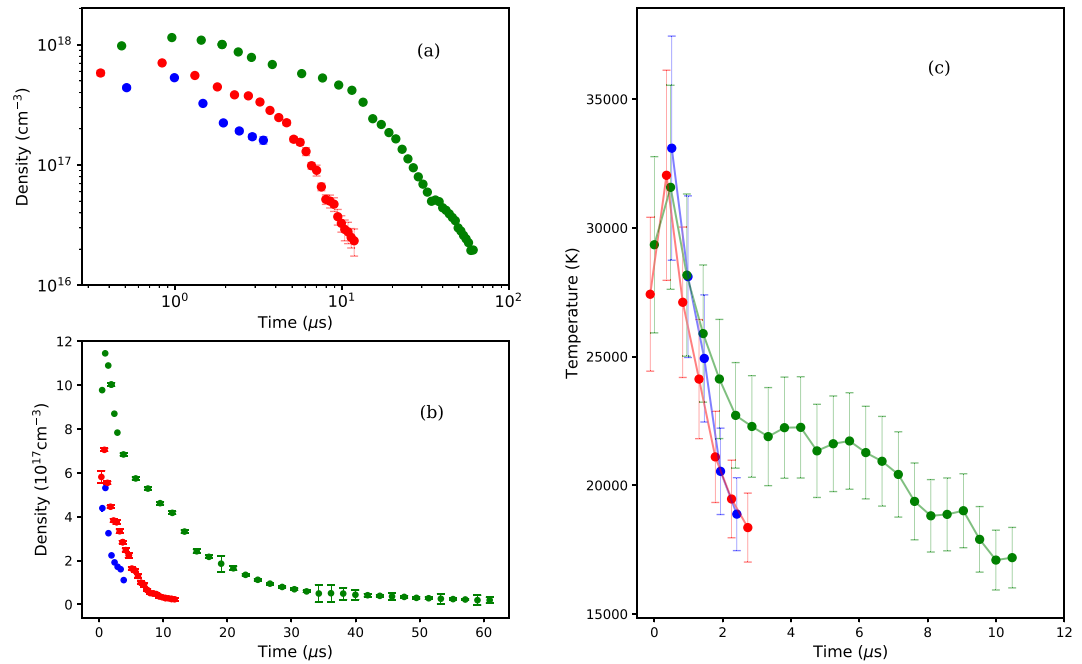
Figure 2. Temporal evolution of the measured electron density in logarithmic (a) and linear (b) scale and temperature (c) for meter long lightning-like discharges (SI, red dots; LI, green dots) and small spark (blue dots) discharges. Due to very weak H_α signal, the electron density could not be measured at $-0.120\,\mu s$ (for the SI discharge) and at $0.000\,\mu s$ (for the LI discharge). Note that the measured electron (gas) temperature values and timescale for the LI discharge (green dots in panel c) are very similar to those reported in natural lightning return strokes (Orville, 1968b) and to those recently reported by Walker and Christian (2019) in triggered lightning return strokes with peak currents of 8.1 kA.

law. The estimation of the error in the electron temperature is evaluated with Equation 11 in Walker and Christian (2019) that depends on the uncertainties in the tabulated Einstein coefficients (Kramida et al., 2019) and in the intensity ratio. The uncertainty in the intensity ratio is calculated using the bootstrap method also adopted above to quantify the error in the electron density.

Figure 2c shows the temperatures for, respectively, the meter long SI (red dots) and LI (green dots) discharges and for the small spark (blue dots). The three discharges analyzed exhibit almost the same maximum temperature of $\simeq 32,000\,K$. The LI discharge (with a peak current of 2.5 kA) is characterized by exhibiting the lowest measured temperatures of $\simeq 16,000\,K$ (after $\simeq 10\,\mu s$). The characteristic timescales of the measured temperatures seem to be connected to the decay times of the currents producing the investigated discharges (tens of microseconds for the LI and $\simeq 1\,\mu s$ for the SI and the small spark). However, the maximum values of the measured temperatures seem to be more related with the similar fast rise times ($\leq 0.5\,\mu s$) of the currents than with the different current peak values. The measured electron temperatures are very similar to those found in natural return strokes (Orville, 1968b) and triggered lightning return strokes with peak currents of 8.1 kA (Walker & Christian, 2019).

6. Exploring Overpressure and Equilibrium Conditions in the Lightning-Like Channel

The equilibrium (LTE) composition of atmospheric pressure lightning-like air plasmas (78% N_2 and 22% O_2) is calculated (see Figures S4–S7) in order to interpret the different features found in the time-resolved spectra of this work and to quantify possible departure from equilibrium.

The equilibrium calculations are performed in the temperature range 1,000–35,000 K with a method based upon the mass action law and the chemical base concept (Godin & Trépanier, 2004; Teulet et al., 2009) and assuming a relative humidity (RH) of 50% that corresponds to the ambient RH measured in the laboratory during experiments. The chemical species considered were 14 atomic, 24 diatomic, and 44 polyatomic
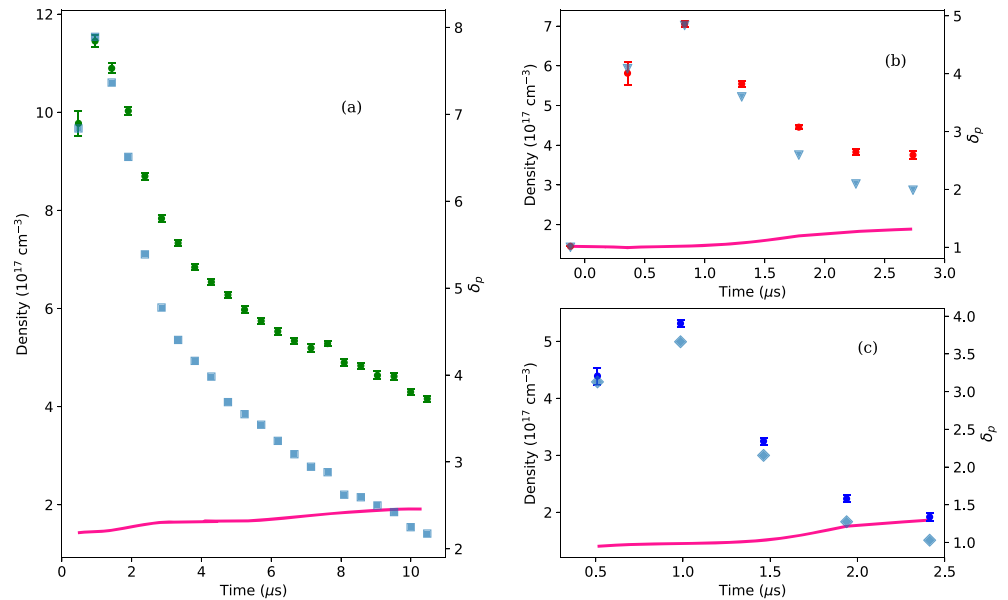
Figure 3. Time dependence of the measured electron density (green, red, and blue dots), calculated equilibrium electron densities (pink solid line) at 1 atm using the measured temperatures, and δ_p (square, triangles, and diamond symbols) quantifying overpressure in discharge channel with respect to ambient pressure ($\delta_p = 1$) for (a) LI mode and (b) SI mode of meter long lightning-like discharges and for (c) a small spark discharge. Note that the measured electron density and the channel overpressure for the LI discharge (panel a) exhibit very similar values to those reported in natural lightning return strokes (Orville, 1968b) and to those recently reported by Walker and Christian (2019) in triggered lightning return strokes with peak currents of 8.1 kA. Regarding panel (b) time $-0.120\,\mu s$ (electron density could not be measured by spectroscopic means at this particular time), note that the SI measured and synthetic spectra agree very well at $-0.120\,\mu s$ (see Figure S11 at 27,000 K and Figure S14). This suggests an equilibrium (at 1 atm) electron density at the pretrigger time of $-0.120\,\mu s$ for the SI discharge shown in (b), which explains why we have included a symbol (diamond) at $-0.120\,\mu s$ for the electron density corresponding to equilibrium air at 1 atm.

species including electrons, negative ions, and single and double positive ions. Internal partition functions were also calculated for atoms, diatomic, and polyatomic molecules as well as for positive and negative ions.

The comparison between the calculated equilibrium and the measured electron densities is shown in Figures 3a–3c for the LI and SI discharge modes and for the small spark. Figure 3 also shows the variation in time of the magnitude $\delta_p = N_e^{\exp}/N_e^{LTE,\ 1\ atm}$ quantifying the overpressure in the discharge channel (while equilibrium is assumed). The values of δ_p change between maxima of $\simeq 8$ (for LI), $\simeq 4.5$ (for SI), and $\simeq 3.5$ (for the small spark) in the posttrigger submicrosecond timescale and minima of roughly $\simeq 2$ (for LI and SI) at $\simeq 10\,\mu s$ (for LI) and at $\simeq 2.73\,\mu s$ (for SI) and $\simeq 1$ (for the small spark) at $\simeq 2.41\,\mu s$.

The comparison of the calculated (equilibrium based at 1 atm) spectra and measured time-resolved spectra (see Figures S11 through S13) reveals that the black-body radiation is negligible (Figure S11) or very weak (Figure S12) in pretrigger times. This is very well illustrated in Figure S11 where synthetic and measured spectra with no black body (very close to optically thin conditions; see Figure S17a) nicely agree at $-0.120\,\mu s$, suggesting that the discharge channel overpressure is still very small and that the electron density in the plasma channel would be very close to the equilibrium electron density at 1 atm (used to compute the synthetic spectra). Interestingly, the black-body continuum suddenly appears at $0.362\,\mu s$ (see Figure S11), and electrons mainly cause overpressure resulting in an optically thicker plasma channel, which measured spectra do not agree with the calculated equilibrium spectra at ambient pressure. We think that this disagreement is mainly due to the fact that the very high speed recorded spectra include light emissions from both the hot core air plasma channel (kept at a lower gas density than ambient) and the hot and overpressure shock front. Right behind the shock front thermal nonequilibrium (different values of translational, vibrational, and electronic temperatures) can occur that could also cause disruption of the Boltzmann equilibrium distribution for sufficiently high shock front speeds as the ones estimated here (Kadochnikov & Arsentiev, 2018).

The overpressure (and the black-body radiation) gradually disappears at $\simeq 2.26\,\mu s$ (see Figure 3b) and the measured and calculated spectra start to exhibit agreement (see Figure S11). Note that, as shown in Figure 3b, $\delta_p \simeq 2.1$ and $\simeq 2.0$ for 2.260 and 2.736 μs (spectra not shown), respectively. The recovery of ambient pressure in the lightning-like plasma channel is more evident at 2.414 μs in the case of the small spark discharge (see Figure S13) where $\delta_p \simeq 1.0$ (see Figure 3c).

Out of the three conditions considered to estimate the temperature in a lightning-like channel, we have investigated two of them (optical thickness and equilibrium). We found that the lightning-like plasma for pretrigger times (only illustrated for the 1-m-long SI mode; see Figure S17a) is close to optically thin and follows Boltzmann equilibrium at 1 atm (see Figure 3b). However, very soon ($\leq 0.5\,\mu s$), it becomes optically thicker, and an overpressure shock front is formed moving outwards very fast. Considering the ambient conditions (RH and air mass density) during our experiments and the total injected electric energy for each investigated discharge (1.2, 81, and 684 J for the small spark and the SI and LI meter long discharges, respectively), we have estimated (see Text S1 and Figures S14–S16) the approximate position (R) and speed (U) of the hydrodynamic shock front resulting from the solution of the Rankine-Hugoniot equations to evaluate the discrete changes in the mass density, pressure, and velocity across the shock front produced after electrical breakdown (Zahn et al., 1982).

The plasma channel gradually returns to optically thin and close to ambient pressure conditions in $\leq 3\,\mu s$ (for SI meter long and small spark discharges) or within several tens of microseconds (for LI meter long discharges). The possible nonequilibrium behind the rapidly moving shock front, the overpressure, and the optical thickness could affect the measurement procedure employed to derive the "temperature" or characteristic energy in the lightning-like channel (see Figure 2c) and could lead to their underestimation.

7. Summary and Conclusion

Submicrosecond high-resolution time-resolved spectra of laboratory-produced lightning-like electrical discharges have been recorded for the first time within the visible spectral range (645–665 nm). Unprecedented spectral time dynamics are explored for meter long and small laboratory electrical discharges.

The maximum electron density and gas temperature measured in a timescale of $\leq 0.50\,\mu s$ (160 ns exposure time) were, respectively, $\simeq 10^{18}\,cm^{-3}$ and $\simeq 32,000\,K$.

Overpressure, equilibrium, and black-body dynamics of the lightning-like plasma channel were investigated. We have computed fast ($>4\,km/s$) propagation speeds for the discharge shock front that, as discussed in previous works (Kadochnikov & Arsentiev, 2018), could lead to the disruption of the Boltzmann equilibrium right behind the shock front in posttrigger submicrosecond times. However, Boltzmann equilibrium was found to be kept at very early pretrigger times (where synthetic spectra based on equilibrium calculations at 1 atm nicely agree with measured spectra) and, depending on the discharge, at "late" times such as $\simeq 2\,\mu s$ (SI and small spark) or $\simeq 10\,\mu s$ (LI) after triggering when the shock front speed has considerably decreased and the pressure inside the discharge channel approaches the ambient one.

Analysis of the temporal evolution of the black-body radiation and of the SA coefficient suggest that meter long discharges and short spark discharges behave differently with respect to the optical thickness of the spectral lines. The optical thickness of meter long discharges is influenced by its overpressure. Close to optically thin lines are found for near ambient pressure channels (occurring at pretrigger and late times). For short sparks, however, the optical thickness of spectral lines seems to change little with time.

A possible slight nonequilibrium just behind the shock wave and a transient partial optical thickness could affect the assumptions underlying the procedure employed to derive the "temperature" in the lightning-like channel and might cause their underestimation.

Future studies will be conducted to investigate real lightning dynamics using submicrosecond time-resolved spectroscopy with GALIUS.

Data Availability Statement

The spectroscopic data presented in this article are available through figshare (at https://bit.ly/2LfG4ay).

References

Bekefi, G. (1976). *Principles of laser plasmas*. New York: John Wiley and Sons.

Cen, J., Yuan, P., Xue, S., & Wang, X. (2015). Spectral characteristics of lightning dart leader propagating in long path. *Atmospheric Research*, *164*, 95–98.

El Sherbini, A., El Sherbini, T. M., Hegazy, H., Cristoforetti, G., Legnaioli, S., & Palleschi, V. (2005). Evaluation of self-absorption coefficients of aluminum emission lines in laser-induced breakdown spectroscopy measurements. *Spectrochimica Acta Part B: Atomic Spectroscopy*, *60*(12), 1573–1579.

Fuquay, D. M., Baughman, R., Taylor, A., & Hawe, R. (1967). Characteristics of seven lightning discharges that caused forest fires. *Journal of Geophysical Research*, *72*(24), 6371–6373.

Gigosos, M. A., González, M. A., & Cardeñoso, V. (2003). Computer simulated Balmer-alpha,-beta and -gamma Stark line profiles for non-equilibrium plasmas diagnostics. *Spectrochimica Acta Part B: Atomic Spectroscopy*, *58*(8), 1489–1504.

Godin, D., & Trépanier, J. (2004). A robust and efficient method for the computation of equilibrium composition in gaseous mixtures. *Plasma Chemistry and Plasma Processing*, *24*(3), 447–473.

Griem, H. (1964). *Plasma spectroscopy*. New York: McGraw-Hill.

Kadochnikov, I., & Arsentiev, I. (2018). Kinetics of nonequilibrium processes in air plasma formed behind shock waves: State-to-state consideration. *Journal of Physics D: Applied Physics*, *51*(37), 374001.

Kramida, A., Yu, R., Ralchenko, Y., Reader, J., & NIST ASD Team (2019). NIST Atomic Spectra Database (ver. 5.7.1). NIST Atomic Spectra Database (ver. 5.7.1) [Online]. Available at https://physics.nist.gov/asd[2020,_January22].NationalInstituteofStandardsand Technology,_Gaithersburg,_MD

Krider, E. P. (1965a). The design and testing of a photoelectric photometer for selected lines in the spectrum of lightning (MS thesis), Univ. of Arizona, Tucson, Arizona.

Krider, E. P. (1965b). Time-resolved spectral emissions from individual return strokes in lightning discharges. *Journal of Geophysical Research*, *70*(10), 2459–2460.

Krider, E. P. (1974). The relative light intensity produced by a lightning stepped leader. *Journal of Geophysical Research*, *79*(30), 4542–4544.

Les Renardieres Group (1981). Negative discharges in long air gaps at Les Renardieres—1978 results and conclusions. *Electra*, *74*. 67–216.

McEachron, K., & Hagenguth, J. (1942). Effect of lightning on thin metal surfaces. *Transactions of the American Institute of Electrical Engineers*, *61*(8), 559–564.

Newman, M., Stahmann, J., Robb, J., Lewis, E., Martin, S., & Zinn, S. (1967). Triggered lightning strokes at very close range. *Journal of Geophysical Research*, *72*(18), 4761–4764.

Nikiforov, A. Y., Leys, C., Gonzalez, M., & Walsh, J. (2015). Electron density measurement in atmospheric pressure plasma jets: Stark broadening of hydrogenated and non-hydrogenated lines. *Plasma Sources Science and Technology*, *24*(3), 34001.

Orville, R. E. (1966a). High-speed, time-resolved spectrum of a lightning stroke. *Science*, *151*(3709), 451–452.

Orville, R. E. (1966b). A spectral study of lightning return strokes (PhD thesis), Univ. of Arizona, Tucson, Ariz.

Orville, R. E. (1968a). A high-speed time-resolved spectroscopic study of the lightning return stroke: Part I. A qualitative analysis. *Journal of the Atmospheric Sciences*, *25*(5), 827–838.

Orville, R. E. (1968b). A high-speed time-resolved spectroscopic study of the lightning return stroke: Part II. A quantitative analysis. *Journal of the Atmospheric Sciences*, *25*(5), 839–851.

Orville, R. E. (1968c). A high-speed time-resolved spectroscopic study of the lightning return stroke: Part III. A time-dependent model. *Journal of the Atmospheric Sciences*, *25*(5), 852–856.

Orville, R. E. (1968d). Spectrum of the lightning stepped leader. *Journal of Geophysical Research*, *73*, 6999.

Orville, R. E. (1975). Spectrum of the lightning dart leader. *Journal of the Atmospheric Sciences*, *32*(9), 1829–1837.

Orville, R. E. (1977). Lightning spectroscopy. In *Lightning: Physics of lightning* (Vol. 1 & 2, p. 281). London: Academic Press.

Orville, R. E., & Salanave, L. E. (1970). Lightning spectroscopy–photographic techniques. *Applied Optics*, *9*(8), 1775–1781.

Parigger, C., Swafford, L., Surmick, D., Witte, M., Woods, A., & Gautam, G. (2014). Hydrogen alpha self-absorption effects in laser-induced air plasma. *Journal of Physics: Conference Series*, *548*, 12043.

Passas, M., Sánchez, J., Kieu, T. N., Sánchez-Blanco, E., & Gordillo-Vázquez, F. J. (2019). GALIUS: An ultrafast imaging spectrograph for the study of lightning. *Applied Optics*, *58*(29), 8002–8006.

Prueitt, M. L. (1963). The excitation temperature of lightning. *Journal of Geophysical Research*, *68*(3), 803–811.

Salanave, L., Orville, R., & Richards, C. (1962). Slitless spectra of lightning in the region from 3850 to 6900 Angstroms. *Journal of Geophysical Research*, *67*(5), 1877–1884.

Teulet, P., Gonzalez, J. J., Mercado-Cabrera, A., Cressault, Y., & Gleizes, A. (2009). One-dimensional hydro-kinetic modelling of the decaying arc in air–PA66–copper mixtures: I. Chemical kinetics, thermodynamics, transport and radiative properties. *Journal of Physics D*, *42*(17), 175201.

Uman, M. A. (1963). The continuum spectrum of lightning. *Journal of Atmospheric and Terrestrial Physics*, *25*(5), 287–295.

Uman, M. A. (1969). Determination of lightning temperature. *Journal of Geophysical Research*, *74*(4), 949–957.

Uman, M. A., & Orville, R. E. (1964). Electron density measurement in lightning from Stark-broadening of H_α. *Journal of Geophysical Research*, *69*(24), 5151–5154.

Walker, T. D., & Christian, H. J. (2017). Triggered lightning spectroscopy: Part 1. A qualitative analysis. *Journal of Geophysical Research: Atmospheres*, *122*, 8000–8011. https://doi.org/10.1002/2016JD026419

Walker, T. D., & Christian, H. J. (2019). Triggered lightning spectroscopy: Part 2. A quantitative analysis. *Journal of Geophysical Research: Atmospheres*, *124*, 3930–3942. https://doi.org/10.1029/2018JD029901

Wang, X., Yuan, P., Cen, J., Liu, J., & Li, Y. (2014). The channel radius and energy of cloud-to-ground lightning discharge plasma with multiple return strokes. *Physics of Plasmas*, *21*(3), 33503.

Warner, T. A., Orville, R. E., Marshall, J. L., & Huggins, K. (2011). Spectral (600–1050 nm) time exposures (99.6 μs) of a lightning stepped leader. *Journal of Geophysical Research*, *116*, D12210. https://doi.org/10.1029/2011JD015663

Zahn, M., Forster, E. O., Kelley, E. F., & Hebner Jr, R. E. (1982). Hydrodynamic shock wave propagation after electrical breakdown. *Journal of Electrostatics*, *12*, 535–546.